Block Krylov Subspace Spectral Methods for Variable-Coefficient Elliptic PDE

James V. Lambers *

Abstract—**Krylov subspace spectral (KSS) methods have been demonstrated to be effective tools for solving time-dependent variable-coefficient PDE. They employ techniques developed by Golub and Meurant for computing elements of functions of matrices to approximate each Fourier coefficient of the solution using a Gaussian quadrature rule that is tailored to that coefficient. In this paper, we apply this same approach to time-independent PDE of the form $Lu = f$, where L is an elliptic differential operator. Numerical results demonstrate the effectiveness of this approach for Poisson's equation and the Helmholtz equation in two dimensions.**

Keywords: ***spectral methods, Gaussian quadrature, block Lanczos method, Poisson's equation, Helmholtz equation***

1 Introduction

Let L be an elliptic second-order differential operator of the form

$$Lu = -\nabla \cdot (p\nabla u) + qu, \tag{1}$$

where $p(x, y) > 0$ and $q(x, y)$ are smooth functions. We consider the following boundary value problem on a rectangle,

$$Lu = g(x, y), \quad 0 < x, y < 2\pi, \tag{2}$$

with homogeneous Dirichlet boundary conditions, or periodic boundary conditions.

In [12] a class of methods, called Krylov subspace spectral (KSS) methods, was introduced for the purpose of solving parabolic variable-coefficient PDE. These methods are based on techniques developed by Golub and Meurant in [3] for approximating elements of a function of a matrix by Gaussian quadrature in the *spectral* domain. In [6, 8], these methods were generalized to the second-order wave equation, for which these methods have exhibited even higher-order accuracy.

It has been shown in these references that KSS methods, by employing different approximations of the solution operator for each Fourier coefficient of the solution, achieve higher-order accuracy in time than other Krylov subspace methods (see, for example, [7]) for stiff systems of ODE, and, as shown in [8], they are also quite stable, considering that they are explicit methods. In [9, 10], the accuracy and robustness of KSS methods were enhanced using block Gaussian quadrature. Recent extensions include the time-dependent Schrödinger equation [11] and Maxwell's equations [14].

It is our hope that by a change of integrand in the integrals used to compute the Fourier coefficients of the solution, the high accuracy achieved for time-dependent problems can be extended to the time-independent case, even for cases in which the operator L is indefinite, as in the Helmholtz equation. Section 2 reviews the main properties of KSS methods, including block KSS methods, and explains how they can be applied to elliptic problems. Numerical results are presented in Section 3, and conclusions are stated in Section 4.

2 Krylov Subspace Spectral Methods

We first review KSS methods, which were first developed in [12] for parabolic problems. Let $S = L^{-1}$ represent the exact solution operator of the problem (2), restricted to one space dimension for simplicity, and let $\langle \cdot, \cdot \rangle$ denote the standard inner product of functions defined on $[0, 2\pi]$,

$$\langle u(x), v(x) \rangle = \int_0^{2\pi} \overline{u(x)} v(x)\, dx. \tag{3}$$

Krylov subspace spectral methods, introduced in [12], use Gaussian quadrature on the spectral domain to compute the Fourier coefficients of the solution. Given the right-hand side $g(x)$, the solution is computed by approximating the Fourier coefficients that would be obtained by applying the exact solution operator to $g(x)$,

$$\hat{u}(\omega) = \left\langle \frac{1}{\sqrt{2\pi}} e^{i\omega x}, Sg(x) \right\rangle. \tag{4}$$

2.1 Elements of Functions of Matrices

In [3] Golub and Meurant describe a method for computing quantities of the form

$$\mathbf{u}^T f(A)\mathbf{v}, \tag{5}$$

where $\mathbf{u}$ and $\mathbf{v}$ are N-vectors, A is an $N \times N$ symmetric positive definite matrix, and f is a smooth function. Our

*Submitted March 20, 2009. Stanford University, Department of Energy Resources Engineering, Stanford, CA 94305-2220 USA Tel/Fax: 650-725-2729/2099 Email: lambers@stanford.edu

goal is to apply this method with $A = L_N$ where L_N is a spectral discretization of L, $f(\lambda) = \lambda^{-1}$, and the vectors $\mathbf{u}$ and $\mathbf{v}$ are derived from $\hat{\mathbf{e}}_\omega$ and $\mathbf{g}$, where $\hat{\mathbf{e}}_\omega$ is a discretization of $\frac{1}{\sqrt{2\pi}} e^{i\omega x}$ and $\mathbf{g}$ represents the right-hand side function $g(x)$, evaluated on an N-point uniform grid.

The basic idea is as follows: since the matrix A is symmetric positive definite, it has real eigenvalues

$$b = \lambda_1 \geq \lambda_2 \geq \cdots \geq \lambda_N = a > 0, \tag{6}$$

and corresponding orthogonal eigenvectors $\mathbf{q}_j$, $j = 1, \ldots, N$. Therefore, the quantity (5) can be rewritten as

$$\mathbf{u}^T f(A)\mathbf{v} = \sum_{j=1}^{N} f(\lambda_j)\mathbf{u}^T \mathbf{q}_j \mathbf{q}_j^T \mathbf{v}. \tag{7}$$

We let $a = \lambda_N$ be the smallest eigenvalue, $b = \lambda_1$ be the largest eigenvalue, and define the measure $\alpha(\lambda)$ by

$$\alpha(\lambda) = \begin{cases} 0, & \text{if } \lambda < a \\ \sum_{j=i}^{N} \alpha_j \beta_j, & \text{if } \lambda_i \leq \lambda < \lambda_{i-1} \\ \sum_{j=1}^{N} \alpha_j \beta_j, & \text{if } b \leq \lambda \end{cases}, \tag{8}$$

where $\alpha_j = \mathbf{u}^T \mathbf{q}_j$ and $\beta_j = \mathbf{q}_j^T \mathbf{v}$. If this measure is positive and increasing, then the quantity (5) can be viewed as a Riemann-Stieltjes integral

$$\mathbf{u}^T f(A)\mathbf{v} = I[f] = \int_a^b f(\lambda)\, d\alpha(\lambda). \tag{9}$$

As discussed in [3], the integral $I[f]$ can be approximated using Gaussian quadrature rules, which yield an approximation of the form

$$I[f] = \sum_{j=1}^{K} w_j f(t_j) + R[f], \tag{10}$$

where the nodes t_j, $j = 1, \ldots, K$, as well as the weights w_j, $j = 1, \ldots, K$, can be obtained using the symmetric Lanczos algorithm if $\mathbf{u} = \mathbf{v}$, and the unsymmetric Lanczos algorithm if $\mathbf{u} \neq \mathbf{v}$ (see [5]).

2.2 Block Gaussian Quadrature

In the case $\mathbf{u} \neq \mathbf{v}$, there is the possibility that the weights may not be positive, which destabilizes the quadrature rule (see [1] for details). One option to get around this problem is rewriting (5) using decompositions such as

$$\mathbf{u}^T f(A)\mathbf{v} = \frac{1}{\delta}[\mathbf{u}^T f(A)(\mathbf{u} + \delta\mathbf{v}) - \mathbf{u}^T f(A)\mathbf{u}], \tag{11}$$

where δ is a small constant. Guidelines for choosing an appropriate value for δ can be found in [12, Section 2.2].

If we compute (5) using (11) or the *polar decomposition*

$$\frac{1}{4}[(\mathbf{u} + \mathbf{v})^T f(A)(\mathbf{u} + \mathbf{v}) - (\mathbf{v} - \mathbf{u})^T f(A)(\mathbf{v} - \mathbf{u})], \tag{12}$$

then we have to carry out the process for approximating an expression of the form (5) with two sets of starting vectors, whereas a single quadrature rule is more desirable. Instead, we consider

$$\begin{bmatrix} \mathbf{u} & \mathbf{v} \end{bmatrix}^T f(A) \begin{bmatrix} \mathbf{u} & \mathbf{v} \end{bmatrix}$$

which results in the 2×2 matrix

$$\int_a^b f(\lambda)\, d\mu(\lambda) = \begin{bmatrix} \mathbf{u}^T f(A)\mathbf{u} & \mathbf{u}^T f(A)\mathbf{v} \\ \mathbf{v}^T f(A)\mathbf{u} & \mathbf{v}^T f(A)\mathbf{v} \end{bmatrix}, \tag{13}$$

where $\mu(\lambda)$ is a 2×2 matrix function of λ, each entry of which is a measure of the form $\alpha(\lambda)$ from (8).

In [3] Golub and Meurant show how a block approach can be used to generate quadrature formulas. We will describe this process here in more detail. The integral $\int_a^b f(\lambda)\, d\mu(\lambda)$ is now a 2×2 symmetric matrix and the most general K-node quadrature formula is of the form

$$\int_a^b f(\lambda)\, d\mu(\lambda) = \sum_{j=1}^{K} W_j f(T_j) W_j + error, \tag{14}$$

with T_j and W_j being symmetric 2×2 matrices. By diagonalizing each T_j, we obtain the simpler formula

$$\int_a^b f(\lambda)\, d\mu(\lambda) = \sum_{j=1}^{2K} f(\lambda_j)\mathbf{v}_j \mathbf{v}_j^T + error, \tag{15}$$

where, for each j, λ_j is a scalar and $\mathbf{v}_j$ is a 2-vector.

Each node λ_j is an eigenvalue of the matrix

$$\mathcal{T}_K = \begin{bmatrix} M_1 & B_1^T & & & \\ B_1 & M_2 & B_2^T & & \\ & \ddots & \ddots & \ddots & \\ & & B_{K-2} & M_{K-1} & B_{K-1}^T \\ & & & B_{K-1} & M_K \end{bmatrix} \tag{16}$$

which is a block-triangular matrix of order $2K$. The vector $\mathbf{v}_j$ consists of the first two elements of the corresponding normalized eigenvector.

To compute the matrices M_j and B_j, we use the block Lanczos algorithm, which was proposed by Golub and Underwood in [4]. Let X_0 be an $N \times 2$ given matrix, such that $X_1^T X_1 = I_2$. Let $X_0 = 0$ be an $N \times 2$ matrix. Then, for $j = 1, \ldots, K$, we compute

$$\begin{aligned} M_j &= X_j^T A X_j, \\ R_j &= A X_j - X_j M_j - X_{j-1} B_{j-1}^T, \\ X_{j+1} B_j &= R_j. \end{aligned} \tag{17}$$

The last step of the algorithm is the QR decomposition of R_j such that X_{j+1} is $n \times 2$ with $X_{j+1}^T X_{j+1} = I_2$. The matrix B_j is 2×2 and upper triangular. The other coefficient matrix M_j is 2×2 and symmetric.

2.3 Block KSS Methods

We are now ready to describe block KSS methods for elliptic PDE in 1-D of the form $Lu = g$. For each wave number $\omega = -N/2+1, \ldots, N/2$, we define

$$R_0(\omega) = \begin{bmatrix} \hat{\mathbf{e}}_\omega & \mathbf{g} \end{bmatrix}$$

and compute the QR factorization $R_0(\omega) = X_1(\omega)B_0(\omega)$. We then carry out the block Lanczos iteration described in (17) to obtain a block tridiagonal matrix $\mathcal{T}_K(\omega)$ of the form (16), where each entry is a function of ω.

Then, we can express each Fourier coefficient of the approximate solution as

$$[\hat{\mathbf{u}}]_\omega = \left[B_0^H E_{12}^H [\mathcal{T}_K(\omega)]^{-1} E_{12} B_0\right]_{12} \tag{18}$$

where $E_{12} = \begin{bmatrix} \mathbf{e}_1 & \mathbf{e}_2 \end{bmatrix}$. The computation of (18) consists of computing the eigenvalues and eigenvectors of $\mathcal{T}_K(\omega)$ in order to obtain the nodes and weights for Gaussian quadrature, as described earlier.

Once the approximation $\mathbf{u}$ is computed using the inverse FFT, we can compute the residual $\mathbf{r} = \mathbf{g} - L_N\mathbf{u}$, and correct the solution by applying the block KSS method again to the problem $L_N\mathbf{c} = \mathbf{r}$, and updating the solution by $\mathbf{u} = \mathbf{u} + \mathbf{c}$. We can continue this process of residual correction until the residual is sufficiently small.

Although we have restricted ourselves to one space dimension in the description of block KSS methods, generalization to higher dimensions is straightforward, as discussed in [13].

3 Numerical Results

In this section we demonstrate the effectiveness of block KSS methods for solving elliptic PDE.

3.1 Poisson's Equation

We first apply a 2-node block KSS method to the problem

$$\nabla \cdot (p(x,y)\nabla u(x,y)) = g(x,y), \quad 0 < x, y < 2\pi, \tag{19}$$

with Dirichlet boundary conditions, where

$$\begin{aligned} p(x,y) \approx\ & 4.03 + 0.017\cos y + 0.0052\sin y + \\ & 0.0026\cos 2y + 0.029\cos x + \\ & 0.014\sin x + 0.0083\cos(x+y) + \\ & 0.0019\cos(x-2y) + \\ & 0.0073\cos(x-y) + \\ & 0.0046\sin(x-y) + 0.0021\cos 2x, \end{aligned} \tag{20}$$

$$\begin{aligned} g(x,y) \approx\ & -2.39\sin y + 1.44\sin 2y + \\ & 0.47\sin 3y - 0.31\sin x - \\ & 1.44\sin(x+y) + 0.19\sin(x+2y) - \\ & 5.73\sin(x-y) - 0.53\sin 2x - \\ & 0.35\sin(2x+y) - \\ & 1.63\sin(2x-y) + 1.07\sin 3x + \\ & 0.6\sin(3x+y). \end{aligned} \tag{21}$$

The coefficient $p(x,y)$ is constructed so as to have the smoothness of a function with four continuous derivatives, using a technique described in [12]. The function f is obtained by applying the spatial operator $Lu = -\nabla \cdot (p\nabla u)$ to a function $u(x,y)$ that is constructed in the same was as $p(x,y)$, with the same smoothness, so that the exact solution is known.

In our experiments, we will use different grid spacings in order to investigate how the error varies with increasing resolution. The problem data is computed on the finest grid, and projected onto the coarser grids. However, in order to isolate error due to KSS methods themselves, we do not include error due to truncation of Fourier series in our error estimates.

The results are shown in Figure 1 and Table 1. The relative error is rapidly reduced by residual correction until it is not much greater than machine precision. As shown in the figure, we achieve linear convergence, with a very small asymptotic error constant. We also see that the error only increases by a factor of 3 as the number of grid points per dimension doubles, but since these error estimates do not include truncation of Fourier series, it follows that the overall error *decreases* as the number of grid points increases.

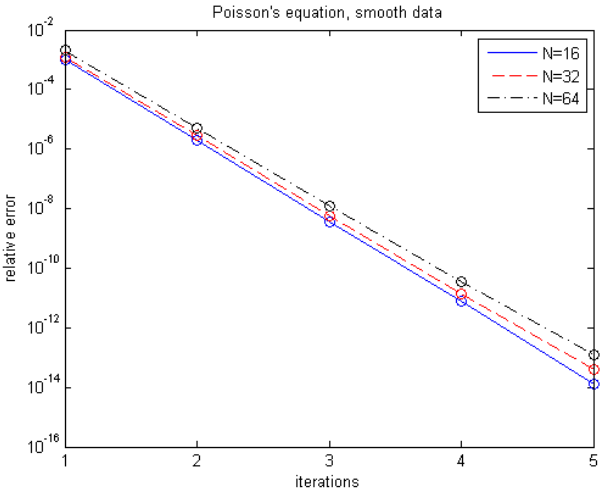

Figure 1: Relative error in solutions to Poisson's equation (19), (20), (21) computed by 2-node block KSS methods with residual correction.

We now solve (19) with a less smooth coefficient and right-hand side,

$$\begin{aligned} p(x,y) \approx\ & 4.04 + 0.017\cos y + 0.0052\sin y + \\ & 0.0089\cos 2y + 0.0042\cos 3y + \end{aligned}$$

Table 1: Relative L^2 error, excluding truncation of Fourier series, in solutions of (19), (20), (21) with N grid points per dimension. The third column lists the number of iterations of residual correction.

N	Error	Iterations
16	1.3e-14	4
32	4.0e-14	4
64	1.2e-13	4

$$
\begin{aligned}
& 0.0021\sin 3y + 0.029\cos x + \\
& 0.014\sin x + 0.0083\cos(x+y) + \\
& 0.0036\cos(x+2y) + 0.0023\cos(x+3y) + \\
& 0.0066\cos(x-2y) + 0.0073\cos(x-y) + \\
& 0.0046\sin(x-y) + 0.0072\cos 2x + \\
& 0.0038\cos(2x+y) + 0.0018\sin(2x+y) + \\
& 0.004\cos(2x-y) - 0.0034\sin(2x-y) + \\
& 0.004\cos 3x + 0.0033\cos(3x+y) + \\
& 0.0026\cos(3x-y), \qquad (22)
\end{aligned}
$$

$$
\begin{aligned}
g(x,y) \approx\ & -2.39\sin y + 4.93\sin 2y + \\
& 3.82\sin 3y - 0.31\sin x - 1.44\sin(x+y) + \\
& 0.68\sin(x+2y) - 1.37\sin(x+3y) - \\
& 0.98\sin(x-3y) - 5.75\sin(x-y) - \\
& 1.78\sin 2x - 1.15\sin(2x+y) - \\
& 1.21\sin(2x+2y) - 1.67\sin(2x+3y) - \\
& 0.24\sin(2x-3y) + 0.95\sin(2x-2y) - \\
& 0.12\cos(2x-y) - 5.47\sin(2x-y) + \\
& 0.34\cos 3x + 8.84\sin 3x + \\
& 0.19\cos(3x+y) + 4.95\sin(3x+y) + \\
& 2.3\sin(3x+2y) - 1.84\sin(3x+3y) + \\
& 0.72\sin(3x-3y) + 0.79\sin(3x-2y) + \\
& 0.98\sin(3x-y), \qquad (23)
\end{aligned}
$$

and with Dirichlet boundary conditions. The results are shown in Figure 2 and Table 2. We observe that even though the Fourier coefficients of the problem data decay more slowly than in the previous problem by two orders of magnitude, the computed solution has comparable accuracy, after just one extra iteration of residual correction. As before, the error increases only moderately as the number of grid points per dimension is doubled.

Figure 3 displays the error in solutions to a one-dimensional analogue of (19) with smoothly varying coefficients and data, after each pass of residual correction, using a 2-node block KSS method with 256 and 512 grid points, respectively. It can easily be seen from the figure, and confirmed by a simple Fourier analysis, that for Poisson's equation, the error in the initial iterations of residual correction is smooth, but becomes less smooth as residual correction continues. Furthermore, the initial

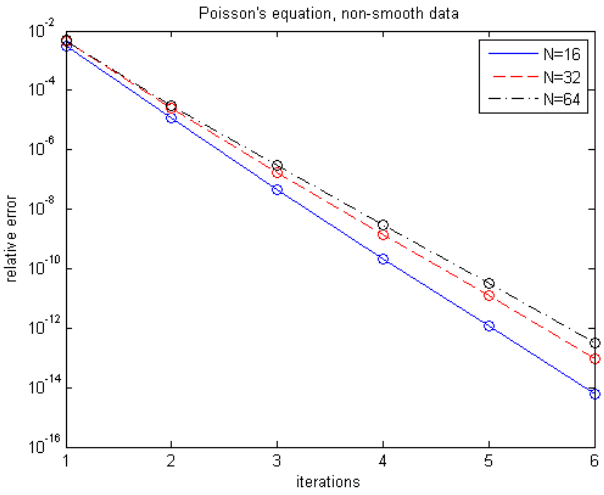

Figure 2: Relative error in solutions to Poisson's equation (19), (22), (23) computed by 2-node block KSS methods with residual correction.

Table 2: Relative L^2 error, excluding truncation of Fourier series, in solutions of (19), (22), (23) with N grid points per dimension. The third column lists the number of iterations of residual correction.

N	Error	Iterations
16	6.0e-15	5
32	8.9e-14	5
64	3.1e-13	5

smooth error is essentially independent of the grid resolution. Therefore, it makes sense to use a multigrid-like approach, in which initial solutions are computed on a coarse grid, and corrected on a finer grid; that is, the opposite sequence of a traditional V-cycle. Future work will explore the development of more efficient iterative methods based on this idea.

3.2 The Helmholtz Equation

Now, we apply a 2-node block KSS method to the inhomogeneous Helmholtz equation

$$\Delta u(x,y) + k(x,y)^2 u(x,y) = g(x,y), \qquad (24)$$

with periodic boundary conditions, where

$$
\begin{aligned}
k(x,y)^2 \approx\ & 4.03 + 0.017\cos y + 0.0052\sin y + \\
& 0.029\cos x + 0.014\sin x + \\
& 0.0083\cos(x+y) + 0.0073\cos(x-y) + \\
& 0.0046\sin(x-y), \qquad (25) \\
g(x,y) \approx\ & 1.63 + 0.015\cos y + 0.0039\sin y + \\
& 0.014\cos x + 0.0057\sin x + \\
& 0.0048\cos(x+y) + 0.0056\cos(x-y) +
\end{aligned}
$$

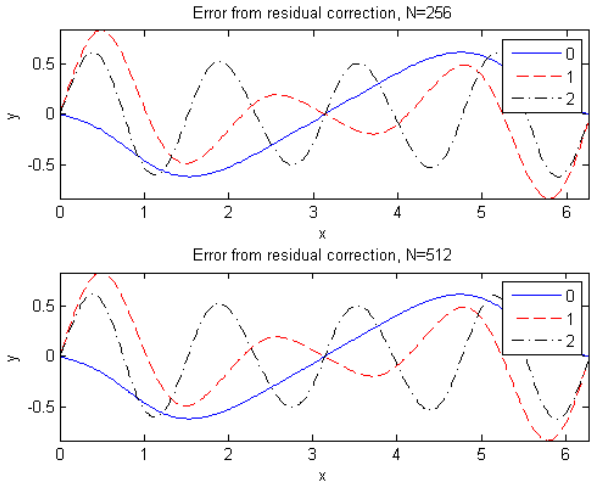

Figure 3: Error in computed solutions to a 1-D analogue of (19) after zero (solid blue curve), one (dashed red curve), two (dotted-dashed black curve) and three (dotted green curve) iterations of residual correction in conjunction with a 2-node block KSS method on a 256-point grid (top plot) and a 512-point grid (bottom plot).

$$0.0033\sin(x-y). \tag{26}$$

The results are shown in Table 3. Although the solution is not as accurate as for Poisson's equation, we note that the accuracy does not degrade with the number of grid points. This is due to the fact that the dominant portion of the error arises from the computation of the Fourier coefficients corresponding to the region of phase space where the symbol of $L = \Delta + k^2$ is smallest. This leads to Gaussian quadrature nodes near the singularity in the integrand $f(\lambda) = \lambda^{-1}$. The integrand is more difficult to approximate accurately by polynomial interpolation near this singularity, and the resulting error is negligibly impacted by the grid refinement.

However, this error is substantially reduced if the coefficient $k(x,y)^2$ and right-hand side $g(x,y)$ are very smooth, because then the basis functions $e^{i\omega\cdot\mathbf{x}}$ are nearly eigenfunctions, which makes most of the terms $\alpha_j\beta_j$ in (8) negligibly small. Future work will explore the use of preconditioning similarity transformations, aided by fast algorithms presented in [2] for application of Fourier integral operators, for homogenizing variable coefficients in order to improve the performance of KSS methods for such problems.

We now solve the modified problem

$$\Delta u(x,y) + 100k(x,y)^2 u(x,y) = g(x,y), \tag{27}$$

with periodic boundary conditions and $k(x,y)$ and $g(x,y)$ as defined in (25), (26). The results are listed in Table 4. We see that even though there is a greater degree of indefiniteness in the operator L, the errors are still quite small, and that high accuracy is achieved after only a single residual correction. This is because the dominant portion of the error, described earlier, corresponds to Fourier coefficients that, in the exact solution, are significantly smaller.

Table 3: Relative L^2 error, excluding truncation of Fourier series, in solutions of (24), (25), (26) with N grid points per dimension. The third column lists the number of iterations of residual correction.

N	Error	Iterations
16	3.5e-9	5
32	3.5e-9	5
64	3.5e-9	5

Table 4: Relative L^2 error, excluding truncation of Fourier series, in solutions of (27), (25), (26) with N grid points per dimension. The third column lists the number of iterations of residual correction.

N	Error	Iterations
16	1.9e-16	1
32	9.7e-15	1
64	1.3e-11	1

We now solve (24) with less smooth coefficients and data,

$$\begin{aligned} k(x,y)^2 \;\approx\;& 4.03 + 0.017\cos y + 0.0052\sin y + \\ & 0.0026\cos 2y + 0.029\cos x + \\ & 0.014\sin x + 0.0083\cos(x+y) + \\ & 0.0019\cos(x-2y) + 0.0073\cos(x-y) + \\ & 0.0046\sin(x-y) + 0.0021\cos 2x, \qquad (28) \\ g(x,y) \;\approx\;& 1.62 + 0.015\cos y + 0.0039\sin y + \\ & 0.0011\cos 2y + 0.014\cos x + \\ & 0.0057\sin x + 0.0048\cos(x+y) + \\ & 0.0056\cos(x-y) + 0.0033\sin(x-y), \qquad (29) \end{aligned}$$

and with periodic boundary conditions. The results are shown in Table 5. We observe that as before, the error is relatively insensitive to increases in the number of grid points per dimension, although the reduced smoothness does cause this error to increase to a small extent.

Finally, we solve the same problem, except that the coefficient k^2 is replaced by $100k^2$. The results are listed in Table 6. We see that the combination of reduced smoothness and the magnitude of the coefficient poses difficulty for block KSS methods as the number of grid points increases. Due to the reduced smoothness, the dominant portion of the error corresponds to Fourier coefficients that are more significant in the exact solution. Furthermore, because these Fourier coefficients correspond

Table 5: Relative L^2 error, excluding truncation of Fourier series, in solutions of (24), (28), (29) with N grid points per dimension. The third column lists the number of iterations of residual correction.

N	Error	Iterations
16	2.6e-7	6
32	1.4e-8	6
64	7.0e-8	6

to higher frequencies than when k^2 is relatively small, higher-frequency oscillations are introduced, which are then amplified by differentiation during the computation of the recursion coefficients in $\mathcal{T}_K$, resulting in larger errors.

Table 6: Relative L^2 error, excluding truncation of Fourier series, in solutions of (27), (28), (29) with N grid points per dimension. The third column lists the number of iterations of residual correction.

N	Error	Iterations
16	3.0e-14	1
32	8.4e-12	1
64	4.5e-5	1

4 Summary and Future Work

We have demonstrated that KSS methods, while originally designed for time-dependent PDE, can also be applied to time-independent elliptic PDE with smoothly varying coefficients. Using residual correction, these methods can compute highly accurate solutions, even for the Helmholtz equation, for which the integrand in the Riemann-Stieltjes integrals used to compute Fourier coefficients is singular.

Future work will extend the approach described in this paper to problems in which the coefficients and data are oscillatory or discontinuous, and problems featuring complicated geometry. In addition, we will consider the use of Gauss-Radau and Gauss-Lobatto rules, in which selected nodes are prescribed, to deal with the singularity associated with the Helmholtz equation. We will also explore the development of multigrid-like approaches to residual correction in order to maximize efficiency.

References

[1] Atkinson, K.: *An Introduction to Numerical Analysis, 2nd Ed.* Wiley (1989)

[2] Candes, E., Demanet, L., Ying, L.: Fast Computation of Fourier Integral Operators. *SIAM J. Sci. Comput.* **29**(6) (2007) 2464-2493.

[3] Golub, G. H., Meurant, G.: Matrices, Moments and Quadrature. *Proceedings of the 15th Dundee Conference*, June-July 1993, Griffiths, D. F., Watson, G. A. (eds.), Longman Scientific & Technical (1994)

[4] Golub, G. H., Underwood, R.: The block Lanczos method for computing eigenvalues. *Mathematical Software III*, J. Rice Ed., (1977) 361-377.

[5] Golub, G. H, Welsch, J.: Calculation of Gauss Quadrature Rules. *Math. Comp.* **23** (1969) 221-230.

[6] Guidotti, P., Lambers, J. V., Sølna, K.: Analysis of 1-D Wave Propagation in Inhomogeneous Media. *Numerical Functional Analysis and Optimization* **27** (2006) 25-55.

[7] Hochbruck, M., Lubich, C.: On Krylov Subspace Approximations to the Matrix Exponential Operator. *SIAM Journal of Numerical Analysis* **34** (1996) 1911-1925.

[8] Lambers, J. V.: Derivation of High-Order Spectral Methods for Time-dependent PDE using Modified Moments. *Electronic Transactions on Numerical Analysis* **28** (2008) 114-135.

[9] Lambers, J. V.: Enhancement of Krylov Subspace Spectral Methods by Block Lanczos Iteration. *Electronic Transactions on Numerical Analysis* **31** (2008) 86-109.

[10] Lambers, J. V.: An Explicit, Stable, High-Order Spectral Method for the Wave Equation Based on Block Gaussian Quadrature. *IAENG Journal of Applied Mathematics* **38** (2008) 333-348.

[11] Lambers, J. V.: Krylov Subspace Spectral Methods for the Time-Dependent Schrödinger Equation with Non-Smooth Potentials. *Numerical Algorithms* in press.

[12] Lambers, J. V.: Krylov Subspace Spectral Methods for Variable-Coefficient Initial-Boundary Value Problems. *Electronic Transactions on Numerical Analysis* **20** (2005) 212-234.

[13] Lambers, J. V.: Practical Implementation of Krylov Subspace Spectral Methods. *Journal of Scientific Computing* **32** (2007) 449-476.

[14] Lambers, J. V.: A Spectral Time-Domain Method for Computational Electrodynamics. *Proceedings of the IAENG Multiconference of Engineers and Computer Scientists* (2009) 2111-2116.